

# Zippering and Entanglement in Flagellar Bundle of *E. Coli*: Role of Motile Cell Body

Tapan Chandra Adhyapak<sup>1,\*</sup> and Holger Stark<sup>1,†</sup>

<sup>1</sup>*Institut für Theoretische Physik, Technische Universität Berlin, Hardenbergstrasse 36, 10623 Berlin, Germany*

(Dated: July 12, 2018)

The course of a peritrichous bacterium such as *E. coli* crucially depends on the level of synchronization and self-organization of several rotating flagella. However, the rotation of each flagellum generates counter body movements which in turn affect the flagellar dynamics. Using a detailed numerical model of an *E. coli*, we demonstrate that flagellar entanglement, besides fluid flow relative to the moving body, dramatically changes the dynamics of flagella from that compared to anchored flagella. In particular, bundle formation occurs through a zipping motion in a remarkably rapid time, affected little by initial flagellar orientation. A simplified analytical model supports our observations. Finally, we illustrate how entanglement, hydrodynamic interactions, and body movement contribute to zipping and bundling.

Understanding self-propulsion of microorganisms pose utmost challenges involving rich and complex physics [1–7]. Bacteria are among the simplest and widely studied of such systems [8–13]. Yet, only recently we are able to explore in full detail the underlying physics involved [14–26]; much of this, however, is still to be apprehended. Propulsion of peritrichous bacteria such as *E. coli* is generated by the rotation of a bundle of several helical propellers, called flagella. Flagella are passive filaments rotated at one end by rotary motors embedded in the cell wall [27]. The level of synchronization and self-organization of rotating flagella crucially decides the swimming course of the cell body, to which they are attached, making it either propel or tumble. However, the dependency is not one-sided: the rotary motors that rotate each flagellum also produce systematic body movements, which in turn affect the flagellar dynamics. While the rotating cell body drags the proximal ends of flagella with it, the distal ends cannot keep up due to friction with the surrounding fluid. In understanding flagellar synchronization and bundling dynamics, focus has so far been given primarily on hydrodynamic interactions and elastic properties of flagella [19, 21, 25, 26, 28, 29]. Although, body movement is speculated to play an important role too [19, 30], knowledge of its detailed impact is still lacking.

The cell body moves in response to the forces and torques acting on it [31]. It translates due to the thrust force generated by the rotating bundle of flagella in the surrounding fluid medium at low Reynolds number. It also has to rotate since the torque on the body has to balance all motor torques acting on the flagella. Ref. [30] argued that the sole effect of body rotation on a flagellum is to simply wrap it around the cell-body axis and thereby enhance bundling. However, real flagella are helical, during tumbling they are more or less arbitrarily oriented [8], and they cannot simply pass through each other. We will demonstrate through our simulations that body rotation in such situations leads to entanglement, where portions of different flagella obstruct each other's free course. While it is well established that hydrodynamic

interactions are sufficient to synchronize [26] and bundle [18, 19, 21] anchored flagella, the role of entanglement for flagellar dynamics is not known so far. In particular, an understanding how cell body motion influences flagellar dynamics is incomplete without considering flagellar entanglement.

In this paper we explore how body movements influences the dynamics of flagella with the help of a realistic numerical model of an *E. coli* that includes detailed flagellar elasticity, hydrodynamic and steric interactions among flagella, and a motile cell body. We demonstrate that body movements dramatically change flagellar behavior leading to profound impacts on the overall dynamics of the cell. In particular, bundle formation happens through flagellar synchronization and a ‘zipping’ motion on an experimental time scale [8], which is much smaller than for anchored flagella [19, 21] and which is approximately independent of the initial orientations of unbundled flagella. We also analyze the relative importance of body movements and flagellar interactions for synchronization and bundling. Our work therefore is a major step towards understanding the propulsion of a peritrichous bacterium close to its real conditions [8, 9].

We first summarize our approach to describe the dynamics of the cell body with multiple flagella in an unbounded fluid of viscosity  $\eta$ . We treat each flagellum as a slender body with centerline  $\mathbf{r}(s)$  parametrized by the arc length  $s$ . By affixing the orthonormal tripod  $\{\mathbf{e}_1(s), \mathbf{e}_2(s), \mathbf{e}_3(s)\}$  at each point on the centerline, where  $\mathbf{e}_3$  is the local tangent and  $\mathbf{e}_1$  and  $\mathbf{e}_2$  are unit vectors along the principal axes of the flagellar cross section, one can fully characterize the bent and twisted flagellum. Dynamics of the flagellum now is governed by Langevin equations for  $\mathbf{r}(s)$  and the twist angle  $\phi(s)$  about the centerline [17]:

$$\partial_t \mathbf{r} = \boldsymbol{\mu}_t (\mathbf{F}_{\text{el}} + \mathbf{F}_s + \mathbf{F}_{\text{th}}) + \mathbf{v}_h, \quad (1)$$

$$\partial_t \phi = \mu_r (T_{\text{el}} + T_{\text{th}}), \quad (2)$$

Here, we separate the velocity contribution  $\mathbf{v}_h$  due to hydrodynamic interactions from local terms and denote local forces and torques by  $\mathbf{F}$ 's and  $T$ 's, respectively.

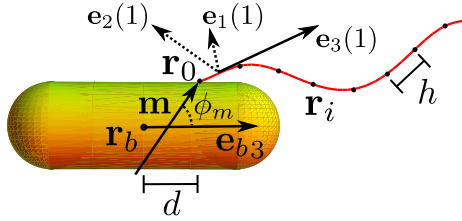


FIG. 1. Schematics of the cell body and part of one flagellum. For clarity, length  $h$  between discretization points  $r_i$  is out of proportion and only the first material tripod  $\{\mathbf{e}_1(1), \mathbf{e}_2(1), \mathbf{e}_3(1)\}$  is shown. The cell body is centered at  $\mathbf{r}_b$  and oriented along the vector  $\mathbf{e}_{b3}$ . The flagellum is attached at  $\mathbf{r}_0$  off-centered by a distance  $d$  along  $\mathbf{e}_{b3}$ . The motor torque drives a tripod at  $\mathbf{r}_0$ .

Self-mobilities  $\boldsymbol{\mu}_t = \mathbf{e}_3 \otimes \mathbf{e}_3 / \gamma_{\parallel} + (\mathbf{I} - \mathbf{e}_3 \otimes \mathbf{e}_3) / \gamma_{\perp}$  and  $\mu_r = 1 / \gamma_R$  are expressed in terms of friction coefficients per unit length. For the flagellum of an *E. coli* they are  $\gamma_{\parallel} = 1.6 \times 10^{-3} \text{pNs} / \mu\text{m}^2$ ,  $\gamma_{\perp} = 2.8 \times 10^{-3} \text{pNs} / \mu\text{m}^2$  and  $\gamma_R = 1.26 \times 10^{-6} \text{pNs}$  [20]. Thermal forces  $\mathbf{F}_{\text{th}}$  and torques  $T_{\text{th}}$  are shown for completeness. Although these are predicted to play an important role during rotation-induced polymorphic transformations of a flagellum [20], they are negligible in our present study [21] and are ignored.

Elastic forces and torques  $\mathbf{F}_{\text{el}} = -\delta\mathcal{F} / \delta\mathbf{r}$  and  $T_{\text{el}} = -\delta\mathcal{F} / \delta\phi$  are derived, respectively, from the total elastic free energy  $\mathcal{F}[\mathbf{r}(s), \phi(s)]$  of the flagellum, the form of which is obtained as follows. The rotational strain vector  $\boldsymbol{\Omega}$  moves the material tripod along the flagellum:  $\partial_s \mathbf{e}_{\nu} = \boldsymbol{\Omega} \times \mathbf{e}_{\nu}$ ;  $\nu = 1, 2, 3$ . Therefore, its components completely characterize the instantaneous flagellar conformation [20]. A small deformation  $d\boldsymbol{\Omega} = \boldsymbol{\Omega} - \boldsymbol{\Omega}^0$  from the normal helical ground state  $\boldsymbol{\Omega}^0 = \{0.0, 1.3, -2.1\}$  [17, 32] needs the Kirchhoff elastic free energy density [33],  $f_k(\boldsymbol{\Omega}) = (A/2)[(d\Omega_1)^2 + (d\Omega_2)^2] + (C/2)(d\Omega_3)^2$ . For *E. coli*, we choose an isotropic bending rigidity  $A = 3.5 \text{pN}\mu\text{m}^2$  (assuming a circular flagellar cross section) and the twist rigidity  $C = A$  [9]. Integrating over the length of the flagellum, we obtain  $\mathcal{F}[\mathbf{r}(s), \phi(s)] = \int ds (f_k + f_{\text{st}})$ , where we include a stretching free energy density  $f_{\text{st}} = K(\partial_s \mathbf{r})^2 / 2$  with  $K = 10^3 \text{pN}$  [17].

To proceed, we discretize Eqs. (1) and (2) by considering discrete positions  $\mathbf{r}_i \equiv \mathbf{r}(s_i)$  along each flagellum and by assigning  $\{\mathbf{e}_1(i), \mathbf{e}_2(i), \mathbf{e}_3(i)\}$  to the straight segment of length  $h$  between  $\mathbf{r}_{i-1}$  and  $\mathbf{r}_i$  (see Fig. 1). Excluded-volume interactions among flagella are enforced by the steric force  $\mathbf{F}_s(\mathbf{r}_i) = \sum_j \mathbf{F}_s^j (h - h_j) / h$ . Here, the summation runs over all overlaps occurring within  $[\mathbf{r}_{i-1}, \mathbf{r}_{i+1}]$  of a given flagellum and  $\mathbf{F}_s^j$  is the steric force at a distance  $h_j < h$  from  $\mathbf{r}_i$ , appropriately decomposed to act on the discrete points (for details see the supplemental material [34]).  $\mathbf{F}_s^j$  derives from the Lennard-Jones potential  $U_{LJ}(r_m) = (F_0 \sigma / 6)[(\sigma / r_m)^{12} - (\sigma / r_m)^6] \Theta(2^{1/6} \sigma - r_m)$ . We truncate it at the minimum using the heaviside step

function  $\Theta(x)$ , where  $r_m$  is the minimal distance between the approaching two flagellar centerlines and  $F_0$  is the strength of the steric force at  $r_m = \sigma$ . We choose  $F_0 = 0.8 \text{pN}$  and adjust  $\sigma = 4a$ , with  $a$  the cross-sectional radius of the flagellar filament, ensuring numerical stability during entanglement in all situations.

Finally, to include hydrodynamic interactions between the flagella, we treat each discrete point  $\mathbf{r}_i$  as a sphere of radius  $a$  and set  $\mathbf{v}_h(\mathbf{r}_i) = \sum_{j \neq i} \boldsymbol{\mu}_{ij} \mathbf{F}(\mathbf{r}_j)$ . Here,  $\boldsymbol{\mu}_{ij}$  is the Rotne-Prager mobility matrix [35] for spheres at  $\mathbf{r}_i$  and  $\mathbf{r}_j$ ,  $\mathbf{F}(\mathbf{r}_j)$  is the local force at  $\mathbf{r}_j$ , and the summation runs over all points of both flagella. We neglect subleading effects from hydrodynamic interactions due to rotation of the spheres. Furthermore, neglecting hydrodynamic lubrication for close flagella is justified for thin filaments and the presence of asperities in real flagella [36].

We model the cell body by a spherocylinder of length  $L_b = 2.5 \mu\text{m}$  and width  $d_b = 0.8 \mu\text{m}$  [27] (see Fig. 1). Point  $\mathbf{r}_0$  of each flagellum is fixed on the body surface and a motor torque  $\mathbf{T}_m = T_m \mathbf{m}$  drives the flagellum by rotating the motor tripod  $\{\mathbf{e}_1(0), \mathbf{e}_2(0), \mathbf{e}_3(0) = \mathbf{m}\}$  at  $\mathbf{r}_0$ . This tripod couples to the main part of the flagellum through the Kirchhoff elastic free energy density  $f_k$ , where we set  $A \rightarrow 0$  and  $C \rightarrow 3C$ . Thus, the driving torque is transferred to the flagellum through a ‘hook’ that acts as an universal joint with low bending and high twist rigidities [37] allowing the first flagellar segment along  $\mathbf{e}_3(1)$  to be at any angle to  $\mathbf{m}$ . In response, the body moves and rotates with velocities  $\mathbf{v}_b = \boldsymbol{\mu}_b^t \mathbf{F}_b$  and  $\boldsymbol{\omega}_b = \boldsymbol{\mu}_b^r (\mathbf{T}_b + \mathbf{T}_m)$ , respectively. Here,  $\mathbf{F}_b$  and  $\mathbf{T}_b$  are the respective force and torque (relative to the body center) resulting from the forces  $\mathbf{F}_{\text{el}} + \mathbf{F}_s$  that act on the flagellar anchoring points. For the mobilities  $\boldsymbol{\mu}_b^t$  and  $\boldsymbol{\mu}_b^r$  we use the analytically available values for a prolate spheroid of aspect ratio  $L_b / d_b$  [38]. The angle  $\phi_m$  between  $\mathbf{m}$  and  $\mathbf{e}_{b3}$  is expected to differ from  $90^\circ$  because of, for example, a locally curved body surface. We adjust  $\phi_m = 55^\circ$  to obtain a ratio for the bundle-to-body rotation within the experimentally observed range [9]. Furthermore, we employ the same potential  $U_{LJ}(r_m)$  to describe the excluded volume interaction between the body and flagella, where  $r_m$  now is the minimal distance between the body surface and any  $\mathbf{r}_i$  on a flagellum.

We now turn to our observations. Fig. 2 shows typical snapshots of the bacterium moving towards the left with the flagella in their normal left-handed helical form. The snapshots were obtained at regular intervals from a particular simulation run. Quantitative details of the corresponding flagellar dynamics are presented in Fig. 3. At time  $t = 0 \text{ms}$ , flagella start with an angle  $\Phi$  between their axes. As time progresses, they rotate counterclockwise about their axes (as viewed from behind the cell) when driven by a positive motor torque  $T_m = 3.4 \text{pN}\mu\text{m}$  [9, 17]. Simultaneously, the cell body performs a counterbalancing clockwise rotation and also translates because of the thrust force generated by the flagella. The resul-

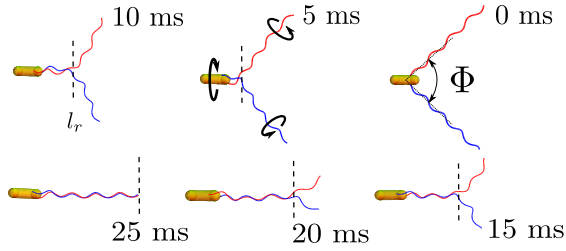


FIG. 2. As the bacterium moves to the left, the flagella form a bundle of length  $l_r$  similar to a closing zipper. Snapshots at various times  $t$  (in ms) for  $\Phi = 90^\circ$  are shown. Rotation directions of cell body and flagella are depicted.

tant flagellar evolution is complex. It involves entanglement and large bending of flagellar axes. To quantify synchronization of flagellar rotation in such situations, we need to compare the respective tripod vectors  $\mathbf{e}_\nu(i)$  and  $\tilde{\mathbf{e}}_\nu(i)$  from the two flagella at the same flagellar position  $i$ . Therefore, we introduce the effective phase difference  $\theta(i) = \cos^{-1}[\mathbf{e}_1(i) \cdot \tilde{\mathbf{e}}_1^*(i)]/\pi$  with  $\tilde{\mathbf{e}}_1^*(i) = \mathcal{R}[\tilde{\mathbf{e}}_1(i)]$ , where  $\mathcal{R}$  rotates the tangent vectors onto each other [ $\tilde{\mathbf{e}}_3^*(i) = \mathbf{e}_3(i)$ ] about the axis  $\mathbf{e}_3(i) \times \tilde{\mathbf{e}}_3(i)$ . Starting from a non-zero initial value, the contour average  $\langle\theta\rangle$  quickly drops towards zero and the flagella reach a nearly synchronized rotational state after about 10 ms [see Fig. 3(a)]. This is also reflected in the snapshot at 10 ms shown in Fig. 2, where the phases of both flagella clearly match. The initial regime remains unaffected when changing the initial value of  $\langle\theta\rangle$ . It is completely determined by hydrodynamics since steric forces are zero as documented by the inset of Fig. 3(a). The subsequent, almost linear decrease of  $\langle\theta\rangle$  towards full synchronization coincides with bundle formation, which we discuss now.

While cell-body movements only quantitatively change synchronization dynamics, they dramatically influence bundling dynamics compared to the case of anchored flagella [18, 19, 21]. At  $t \sim 10$  ms proximal portions of the flagella start to wrap around the body axis [see Fig. 2], after synchronization has already proceeded considerably. This marks the beginning of bundling near the cell body, while rest of the flagella are still apart. With time the front of the bundled portion advances away from the body, gradually drawing remaining loose flagellar portions into the bundle. The growth of the bundled portion thus resembles a ‘zipping’ motion, where the ‘zip’ starts at a point near the body and continues till whole of the flagella have joined the bundle.

To quantify these findings, we define the bundled portion as the part of a flagellum for which all its points are at distances  $\leq 2R$  from the other flagellum. We choose  $R = 0.22 \mu\text{m}$  to be the equilibrium radius of the helical flagellum. The bundle length  $l_r$  is then measured from the cell body to the bundle front normalized by the axial length  $L_{ax}$  of a flagellum. As seen from Fig. 3(b), ‘zipping’ takes place within approximately 5 - 20 ms. During

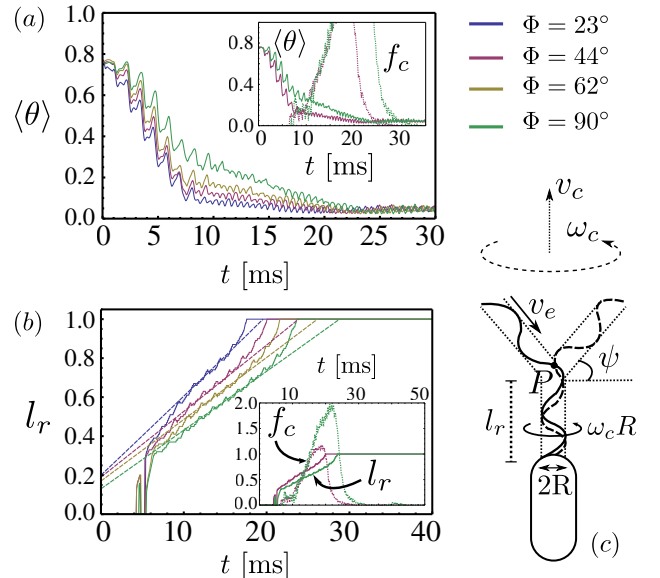


FIG. 3. (a) Contour-averaged phase difference  $\langle\theta\rangle$  plotted versus time  $t$  for various values of the opening angle  $\Phi$ . (b) Bundle length  $l_r$  plotted against  $t$  for the same  $\Phi$ 's obtained from simulations (full lines) and an analytical model (dashed lines). The analytical model fits best for  $R = 0.30 \mu\text{m}$ , when  $v_c = 22.5 \mu\text{m/s}$ ,  $\omega_c/2\pi = 11.4$  Hz,  $\lambda_f = 2.5 \mu\text{m}$ ,  $\nu_f = 83.3$  Hz. (c) Body motion ( $v_c, \omega_c$ ) and flagellar phase velocity  $v_e$  determine the speed of the bundle front  $P$  in the analytical model. Insets: Steric force density  $f_c$  (in  $\text{pN}/\mu\text{m}$ ) correlated with time evolutions of  $\langle\theta\rangle$  in (a) and  $l_r$  in (b), for  $\Phi = 44^\circ$  and  $90^\circ$ .

this period, after an initial sharp increase  $l_r$  grows almost linearly with time. Furthermore, for the studied range of opening angles  $\Phi$  the bundling time only varies by about 10 ms. Therefore, it is always much smaller than the total tumble time of 150 - 450 ms [8]. So, bundling during a tumble event is remarkably independent of the extent to which a flagellum is thrown out of a bundle. This gives a crucial insight into the locomotion of a bacterium since bundling without supporting body movements takes much longer.

Flagellar entanglement is observed to play an important role in all the findings mentioned above. During zipping, the steric force density  $f_c = |\mathbf{F}_s|/L$ , where  $L$  is the length of a flagellum, is found to build up until bundling completes, after which  $f_c$  declines rapidly [inset, Fig. 3(b)]. Due to viscous drag and flagellar flexibility, parts of the flagella not in the bundle hardly follow the cell-body rotation (see movie M1 in the Supplemental material [34]). As a result, proximal portions of the flagella not only start to wrap around the body axis but also get entangled [snapshot at  $t = 10$  ms, Fig. 2]. This drastically enhances flagellar bundling: further rotation of proximal ends is possible only when the entangled front proceeds away from the body, gradually bringing the rest of the flagella quickly into the bundle. A simplified ana-

lytical model discussed below further supports these observations. A correlation between  $f_c$  and the slow linear decline of  $\langle\theta\rangle$  mentioned earlier is clear from the inset of Fig. 3(a). While flagella in the bundle are synchronized, the local phase differences  $\theta(i)$  of their free ends fluctuate strongly until entanglement forces them into the bundle. This is observed to be responsible for the delayed slow decline of  $\langle\theta\rangle$ .

A simplified model for the zipping dynamics takes into account flagellar entanglement at the bundle front and fluid flow in the body-fixed reference frame. The latter occurs with respective translational and rotational velocities  $\mathbf{v}_c = -\mathbf{v}_b$  and  $\boldsymbol{\omega}_c = -\boldsymbol{\omega}_b$  [see Fig. 3(c)]. Accordingly, the length of the bundle grows with speed  $dl_r/dt$  and the angle  $\psi = 90^\circ - \Phi/2$  varies in time according to

$$\frac{dl_r}{dt} = v_e + \frac{\omega_c R}{\cos \psi} \quad \text{and} \quad \frac{d\psi}{dt} = \frac{v_c \cos \psi}{L_{ax} - l_r}. \quad (3)$$

Like in a zipper the free portions of the rotating flagella are dragged into the bundle front  $P$  with the helical phase velocity  $v_e$ . They are perfectly fit into the bundle; hence  $l_r$  grows with the same speed  $v_e = \lambda_f \nu_f$ , where  $\lambda_f$  is the helical pitch and  $\nu_f$  the frequency of rotation. Second, the surrounding fluid wraps the free flagellar portions with an angular velocity  $\omega_c$  onto the bundle cylinder. So, flagella are dragged with an additional speed  $\omega_c R / \cos \psi$  into the bundle front, where  $R$  is an effective bundle radius. Finally, the translational flow rotates the flagellar tip with speed  $v_c \cos \psi$  about the bundle front  $P$ , which gives the angular velocity  $d\psi/dt$ . Eqs. (3) are solved for  $l_r(t)$  using parameter values measured from our simulations with  $R$  and  $l_r(t=0)$  adjusted for the best fit. The results plotted as dashed lines in Fig. 3(b) agree well with our simulation results, strengthening the interpretation of our observations discussed above.

To obtain further insight into flagellar dynamics, we make a comparative study to judge the relevance of cell-body movements and various flagellar interactions. The results are presented in Fig. 4. We consider the standard simulation run performed at  $\Phi = 23^\circ$ . Its results [curves (i) in Fig. 4] are compared with those obtained from new simulations where either body movements or flagellar interactions are ignored. The impact of body rotation on the synchronization dynamics is more pronounced than that of body translation [inset, curves (iii) and (iv)]. Without body rotation,  $\langle\theta\rangle$  converges more slowly towards zero, qualitatively resembling the results of anchored flagella [26]. However, absence of body translation does not affect the outcome much. Hydrodynamic interactions (HI) between flagella are important in reproducing the standard result of the full simulation [inset, curves (i) and (ii)]. However, we find that synchronization is even possible without HI contrasting the situation of anchored flagella, where HI between flagella are known to be essential [26]. Interestingly, cell-body movement is sufficient to synchronize flagella, similar to findings for

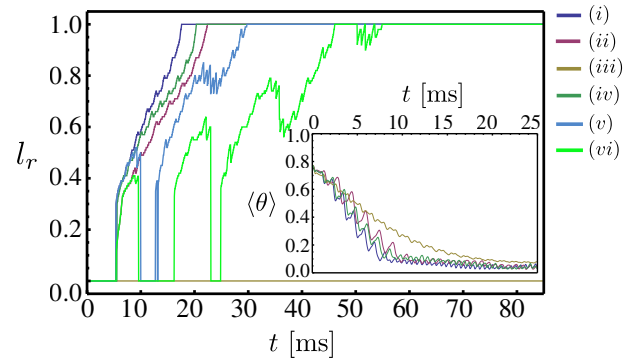


FIG. 4. Comparison of different factors affecting bundling and synchronization dynamics (inset). Curves (i): standard simulation run performed for  $\Phi = 23^\circ$ ,  $\theta(i) = 0.8 \forall i$ , and  $T_m = 3.4 \text{ pN}\mu\text{m}$ . Other curves show simulation runs that ignore: (ii) hydrodynamic interactions among flagella, (iii) axial body rotation, (iv) body translation, (v) steric interaction between flagella, or (vi) both steric and hydrodynamic interactions.

*Chlamydomonas* in Ref. [39].

Bundling dynamics is affected with a similar trend. While bundling is delayed by ca. 10 ms in absence of HI between flagella, absence of body translation is less severe [curves (i), (ii), and (iv) in Fig. 4]. There is no bundle formation in absence of axial body rotation [horizontal line as curve (iii)] because the body re-orientates and slows down translation, resulting in an unusual buckling of flagella away from each other. More significantly, when we follow Ref. [30] and allow temporal evolution of each flagella affected only by body movement but not by either HI or steric interactions, bundling gets significantly delayed by about 30 ms [curves (v) and (vi)].

To conclude, we present a detailed modeling of an *E. coli* with two flagella and a motile cell body. This allows us to probe bacterial propulsion on an yet experimentally inaccessible level. The complex role of flagellar polymorphism is ignored for simplicity. In principle, it can be probed extending our model [17]. We demonstrate that compared to the situation of anchored flagella, flagellar dynamics close to real conditions is strikingly altered by body movements. Times to bundle and synchronize are dramatically reduced. In particular, flagellar entanglement helps bundling to proceed quickly like a ‘zipping’ motion, which we rationalize in a simplified model. Furthermore, we demonstrate that body movement and flagellar entanglement lead to rapid bundling and synchronization even when hydrodynamic interactions are neglected. Our findings are important in explaining experimentally observed times scales as mentioned above.

Finally, more and more artificial microswimmers using different swimming mechanisms have been and are constructed [40]. We provide here an example how one develops a model for exploring and ultimately understanding the biomechanics of microswimmers.

We are grateful to R. Vogel for useful discussions and providing key insights to the numerics involved. We also acknowledge D. Alizadehrad, G. Gompper, P. Kanehl, O. Pohl, C. Prohm, R. Winkler, and A. Zöttl for helpful discussions. We thank the VW foundation for financial support within the program “Computational Soft Matter and Biophysics” (Grant No. I/86 801).

---

\* [tapan.c.adhyapak@tu-berlin.de](mailto:tapan.c.adhyapak@tu-berlin.de)

† [holger.stark@tu-berlin.de](mailto:holger.stark@tu-berlin.de)

- [1] M. Ramia, D. Tullock, and N. Phan-Thien, *Biophys. J.* **65**, 755 (1993).
- [2] E. Lauga and T. R. Powers, *Rep. Prog. Phys.* **72**, 096601 (2009).
- [3] R. Cortez, L. Fauci, and A. Medovikov, *Phys. Fluids* **17**, 031504 (2005).
- [4] J. Saragosti, V. Calvez, N. Bournaveas, B. Perthame, A. Buguin, and P. Silberzan, *Proc. Natl. Acad. Sci.* **108**, 16235 (2011).
- [5] B. Rodenborn, C.-H. Chen, H. L. Swinney, B. Liu, and H. P. Zhang, *Proc. Natl. Acad. Sci.* **110**, E338E347 (2013).
- [6] S. P. Strong, B. Freedman, W. Bialek, and R. Koberle, *Phys. Rev. E* **57**, 4604 (1998).
- [7] D. Alizadehrad, T. Krüger, M. Engstler, and H. Stark, *PLoS Comput. Biol.* **11**, e1003967 (2015).
- [8] L. Turner, W. S. Ryu, and H. C. Berg, *J. Bacteriol.* **182**, 2793 (2000).
- [9] N. C. Darnton, L. Turner, S. Rojevsky, and H. C. Berg, *J. Bacteriol.* **189**, 1756 (2007).
- [10] R. M. Macnab and M. K. Ornston, *J. Mol. Biol.* **112**, 1 (1977).
- [11] R. M. Macnab, *Annu. Rev. Microbiol.* **57**, 77 (2003).
- [12] D. S. H. Shah, T. Pehinec, S. M. Stevens, S.-I. Aizawa, and R. E. Sockett, *J. Bacteriol.* **182**, 5218 (2000).
- [13] J. P. Armitage and R. M. Macnab, *J. Bacteriol.* **169**, 514 (1987).
- [14] M. Kong, Y. Wu, G. Li, and R. G. Larson, *Soft Matter* **11**, 1572 (2015).
- [15] J. H. Tu, M. Arcak, and M. M. Maharbiz, *Phys. Rev. E* **91**, 023018 (2015).
- [16] P. Kanehl and T. Ishikawa, *Phys. Rev. E* **89**, 042704 (2014).
- [17] R. Vogel and H. Stark, *Phys. Rev. Lett.* **110**, 158104 (2013).
- [18] S. Y. Reigh, R. G. Winkler, and G. Gompper, *PLoS ONE* **8**, e70868 (2013).
- [19] S. Y. Reigh, R. G. Winkler, and G. Gompper, *Soft Matter* **8**, 4363 (2012).
- [20] R. Vogel and H. Stark, *Eur. Phys. J. E* **35**, 15 (2012).
- [21] P. J. A. Janssen and M. D. Graham, *Phys. Rev. E* **84**, 011910 (2011).
- [22] N. Watari and R. G. Larson, *Biophys. J.* **98**, 12 (2010).
- [23] C. Speier, R. Vogel, and H. Stark, *Phys. Biol.* **8**, 046009 (2011).
- [24] H. Wada and R. R. Netz, *Europhys. Lett.* **82**, 28 001 (2008).
- [25] H. Flores, E. Lobaton, S. Mndez-Diez, S. Tlupova, and R. Cortez, *Bull. Math. Biol.* **67**, 137 (2005).
- [26] M. Reichert and H. Stark, *Eur. Phys. J. E* **17**, 493 (2005).
- [27] H. Berg, *E. coli in Motion* (Springer, New York, 2004).
- [28] M. Kim, J. C. Bird, A. J. Van Parys, K. S. Breuer, and T. R. Powers, *Proc. Natl. Acad. Sci.* **100**, 15481 (2003).
- [29] M. Kim and T. R. Powers, *Phys. Rev. E* **69**, 061910 (2004).
- [30] T. R. Powers, *Phys. Rev. E* **65**, 040903 (2002).
- [31] E. M. Purcell, *Proc. Natl. Acad. Sci.* **94**, 11307 (1997).
- [32] C. Calladine, *J. Theoret. Biol.* **57**, 469 (1976).
- [33] L. D. Landau and E. M. Lifshitz, *Theory of Elasticity* (Pergamon, New York, 1986).
- [34] See Supplemental Material at [URL will be inserted by publisher] for the detailed numerical scheme to calculate the steric forces and for the movie M1 showing the synchronization and bundling of two flagella attached to a motile cell-body.
- [35] J. Dhont, *An Introduction to Dynamics of Colloids* (Elsevier Science B.V, Amsterdam, 1996).
- [36] R. Sundararajakumar and D. L. Koch, *J. Non-Newtonian Fluid Mech.* **73**, 205 (1997).
- [37] K. Namba and F. Vonderviszt, *Q. Rev. Biophys.* **30**, 1 (1997).
- [38] S. Kim and S. Karilla, *Microhydrodynamics: Principles and Selected Applications* (Dover Publications, New York, 2005).
- [39] B. M. Friedrich and F. Jüllicher, *Phys. Rev. Lett.* **109**, 138102 (2012).
- [40] R. Dreyfus, J. Baudry, M. Roper, H. Stone, M. Fermigier, and J. Bibette, *Nature* **437**, 862 (2005); A. Ghosh and P. Fischer, *Nano Lett.* **9**, 2243 (2009); L. Zhang, J. J. Abbott, L. Dong, B. E. Kratochvil, D. Bell, and B. J. Nelson, *Appl. Phys. Lett.* **94**, 064107 (2009).